# CHAPTER IV

# RESULTS AND DISCUSSION

This chapter consists of results from calculations performed during the data analysis, focusing on the outcomes of the model simulation.

## 4.1 Time evolution in light nuclei multiplicities

After the extraction of the light nuclei in which we are interested in, we can now plot the time evolution of their multiplicities within the spatial volume compared to the multiplicities at midrapidity $|y| < 0.50$ for beam energies of $2.0$ $A$GeV and $3.0$ $A$GeV (see figures 4.1-4.2).

Figure 4.1 presents the time evolution of light nuclei multiplicities at beam energies of $2.0$ $A$GeV (averaged over 64,000 events) and $3.0$ $A$GeV (averaged over 80,000 events). In the early and late stages of the reaction, the multiplicities in both the first-order phase transition and crossover scenarios exhibit minimal differences. However, during the interval corresponding to the co-existence phase, approximately between 8 and 24 fm/c, the average baryon density attained in the first-order phase transition case exceeds that of the crossover. This enhanced density within a fixed central spatial volume leads to an increased net baryon number and yields of the light nuclei within the same region.

On the contrary, the evolution in momentum space shows no differences between the crossover and phase transition scenarios, with yields being almost identical for all examined particle species. This indicates that phase transition primarily influences the spatial configuration of baryons in the dense phase, while having little impact on momentum space fluctuations.

## 4.2 Time evolution in cumulant ratios of the light nuclei

It is now interesting to explore whether a phase transition has an impact on baryon number fluctuations and, in turn, on correlations in phase space. To investigate this, we study how the cumulant ratios defined in Eq. (13) change over time, beginning with the scaled variance shown in figures 4.3 and 4.4 for beam energies of $E_{\text{lab}} = 2.0$ $A$GeV and $3.0$ $A$GeV (top and bottom panels, respectively).

In coordinate space, we observe that the total baryon number remains conserved, causing the baryon values to start below the Poisson baseline of 1, in contrast to other particles. A significant increase in $\frac{\sigma^2}{\mu}$ is found in the phase transition scenario compared to the crossover, peaking at the moment of maximum compression. Protons exhibit a less pronounced increase, they constitute only a fraction of the total baryon number and are subject to resonance excitations and decays. Nuclear clusters show an even smaller but still noticeable enhancement.

Proceeding to the evolution in the momentum space, minimal differences between the crossover and phase transition scenarios are observed, with particle yields of all species remaining nearly identical. This indicates that phase separation primarily influences the spatial distribution of baryons in the dense phase, while having only a minor impact on fluctuations in the momentum space.

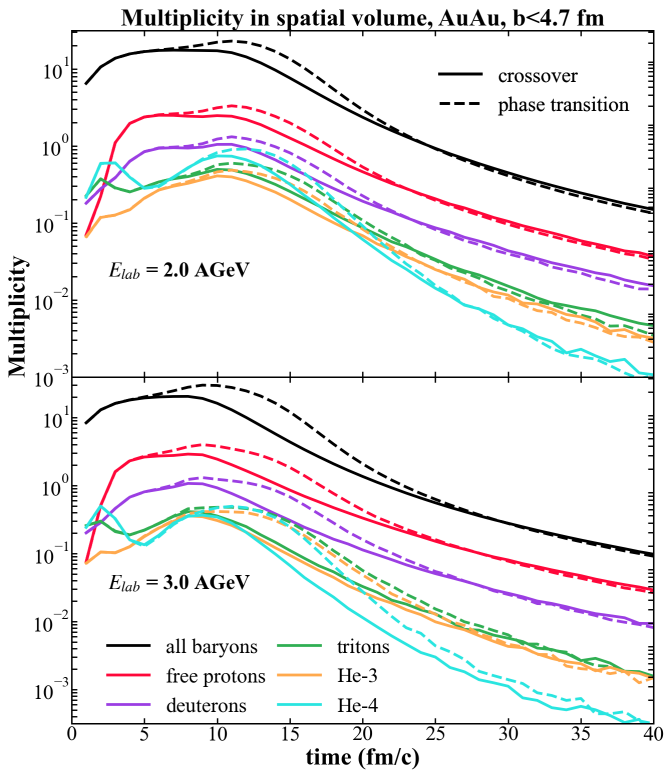


**Figure 4.1** Time evolution in light nuclei multiplicities (proton (red), deuteron (purple), triton (green), $^3He$ (orange), $^4He$ (blue) at $E_{\text{lab}} = 2.0$ $A$GeV (upper plot) and $3.0$ $A$GeV (lower plot). The plots display the multiplicities within the spherical volume with radius 2 fm centered at the origin from UrQMD calculations with phase transition (dashed lines) and with a crossover (solid lines).

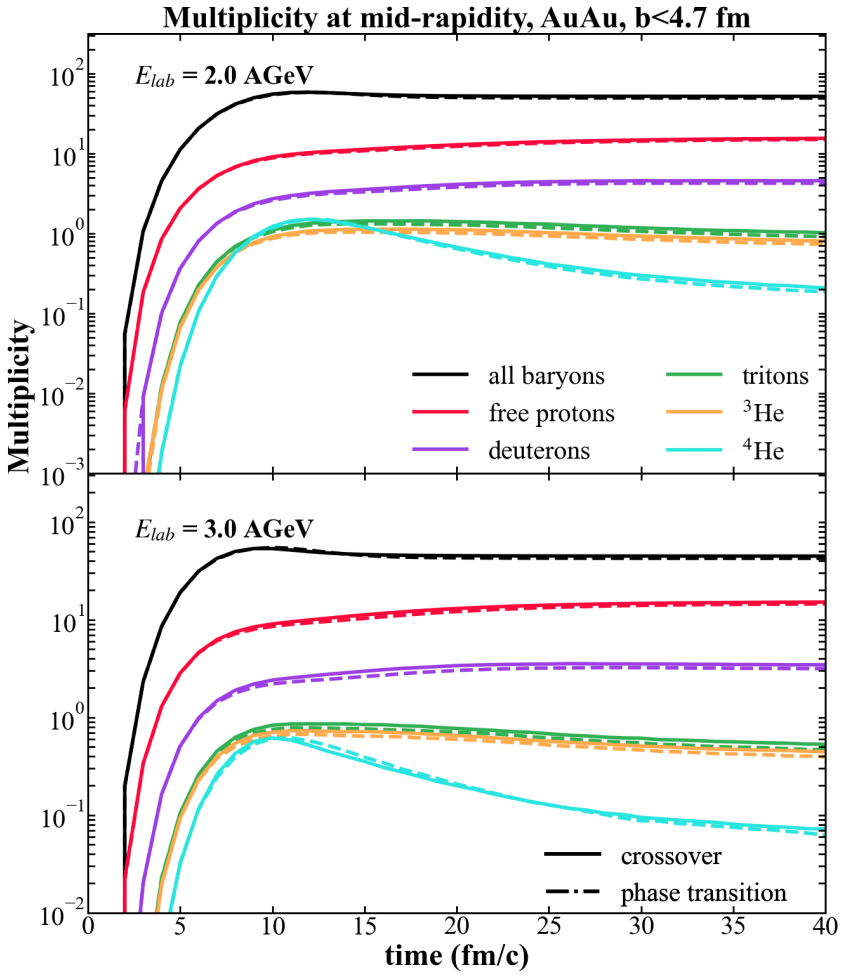


**Figure 4.2** Time evolution in light nuclei multiplicities (proton (red), deuteron (purple), triton (green), $^3He$ (orange), $^4He$ (blue) at $E_{\text{lab}} = 2.0$ $A$GeV (upper plot) and $3.0$ $A$GeV (lower plot). The plots display the multiplicities at mid-rapidity $|y| \leq 0.5$ from the same calculations.

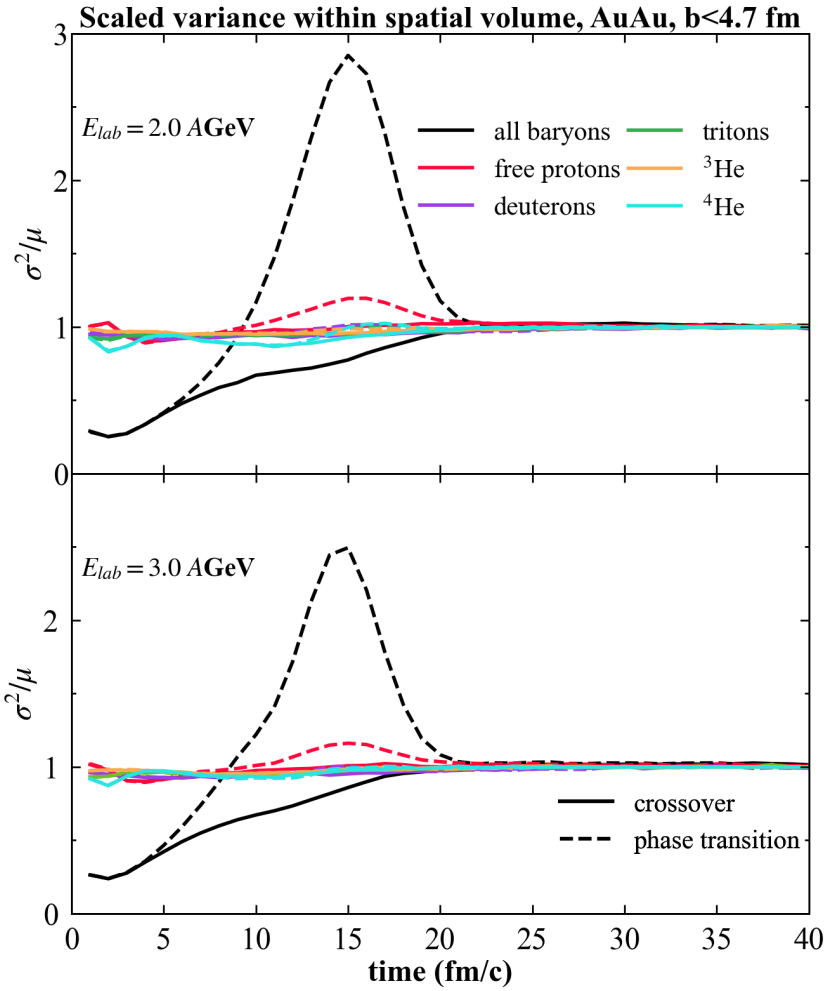


**Figure 4.3** Time evolution of the scaled variance of the multiplicities of baryons (grey), protons (red) and light nuclei (deuterons (purple), tritons (green), $^3He$ (orange), $^4He$ (blue)) at $E_{\text{lab}} = 2.0\ A$GeV (upper plot) and $3.0\ A$GeV (lower plot) within a spatial volume. The UrQMD calculations were carried out using a CMF equation of state (EoS) that includes either a first-order phase transition (dashed lines) or a smooth crossover (solid lines). A distinct enhancement in the baryon cumulants is observed during the phase transition.

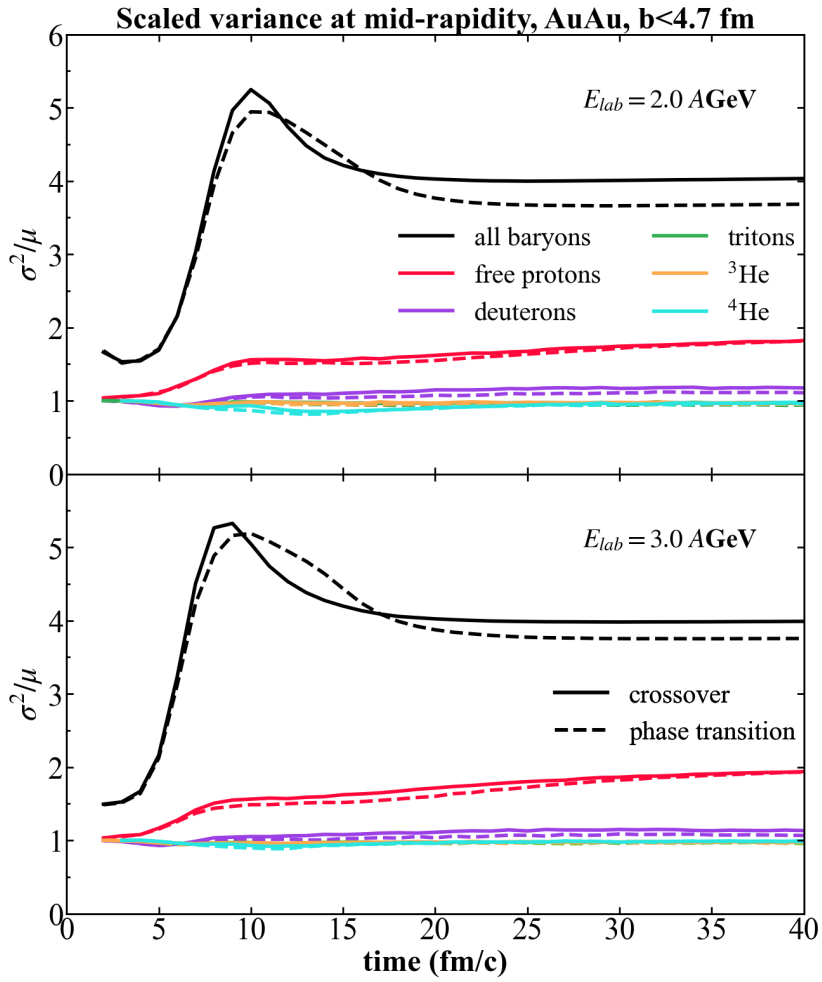


**Figure 4.4** Time evolution of the scaled variance of the multiplicities of baryons (grey), protons (red) and light nuclei (deuterons (purple), tritons (green), $^3He$ (orange), $^4He$ (blue)) at $E_{\text{lab}} = 2.0$ $A$GeV (upper plot) and $3.0$ $A$GeV (lower plot) within the rapidity interval $-0.50 \leq y \leq 0.50$ from the same UrQMD calculations with the phase transition EoS. During the phase transition, free protons and other nuclear clusters are only slightly affected.

The behavior of $S\sigma$ shows a similar tendency, as displayed in figure 4.5. However, a clear discrimination appears at higher energy of $E_{\text{lab}} = 3.0\ A\text{GeV}$, particularly in the lower plot. At this energy, the presence of a phase transition results in a pattern of enhancements, followed by suppression, and then another enhancement in the net-baryon number cumulant, conversely to the smoother behavior seen with a crossover. This pattern arises from the qualitatively different dynamical evolution of the system at two energies. Explicitly, at $E_{\text{lab}} = 3.0\ A\text{GeV}$, the system overshoots into the spinodal region while crossing spinodal lines during its expansion which is not a feature observed at the lower energy.

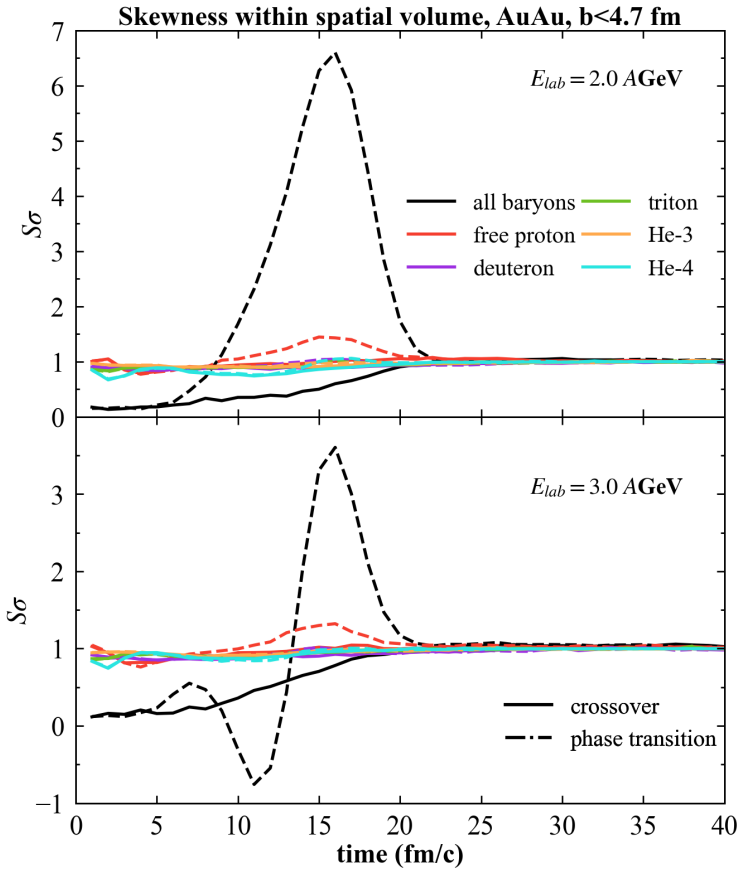


**Figure 4.5** Time evolution of the skewness of the multiplicities of baryons (black), protons (red) and light nuclei (deuterons (purple), tritons (green), $^3He$ (orange), $^4He$) at $E_{\text{lab}} = 2.0\ A\text{GeV}$ (upper plot) and $3.0\ A\text{GeV}$ (lower plot). The plots show the results within a spatial volume. UrQMD calculations were conducted using a CMF EoS incorporating either a first-order phase transition (dashed lines) or a smooth crossover (solid lines).

Correspondingly to the scaled variance, the evolution in momentum space of $S\sigma$ does not exhibit a clear distinction between the two scenarios. Although a late-time suppression of $S\sigma$ is also observed at $2.0$ $A$GeV, the effect is considerably weaker at $3.0$ $A$GeV (see figure 4.6). This aligns with previous findings indicating that volume fluctuations have a greater impact on second-order cumulants than on third-order ones (Bzdak, Koch and Skokov, 2017).

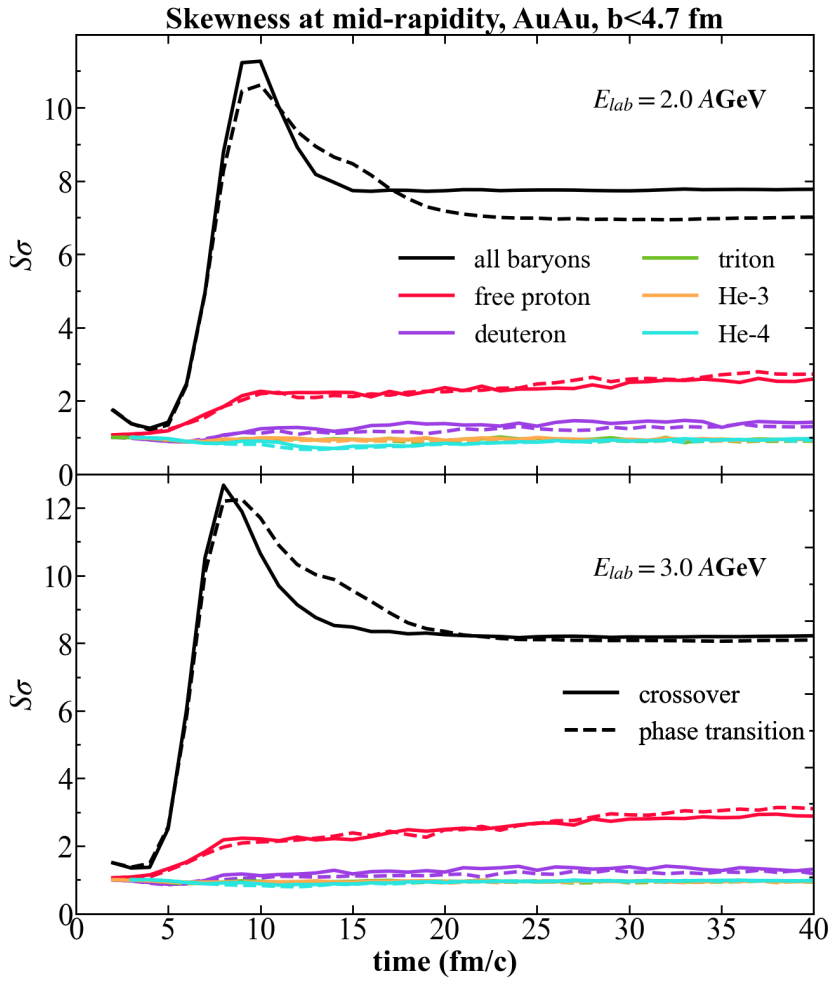


**Figure 4.6** Time evolution of the skewness of the multiplicities of baryons (black), protons (red) and light nuclei (deuterons (purple), tritons (green), $^3He$ (orange), $^4He$) at $E_{\text{lab}} = 2.0$ $A$GeV (upper plot) and $3.0$ $A$GeV (lower plot). The plots show the results within the rapidity range $|y| \leq 0.50$ from the same UrQMD calculations with the phase transition EoS.

## 4.3 Cumulant ratios in different rapidity windows

Although no significant signal is observed in the momentum space, it remains crucial to determine the optimal choice of rapidity acceptance window for experimentally studying cumulant ratios. Therefore, we examine how the cumulants for baryons, deuterons, and free protons vary with the width of the rapidity window.

The rapidity window is defined by $\Delta y = y_{max} - y_{min}$ where $y_{max}$ and $y_{min}$ are maximum and minimum rapidity, respectively, with $y_{min} = -y_{max}$ and $y_{max} > 0$. We have chosen rapidity windows at two fixed time steps of 8 fm/c and 50 fm/c to compare fluctuations in the initial and late stage of the collision for the corresponding cumulant ratios: the scaled variance $\frac{\sigma^2}{\mu}$ which is available in figures 4.7-4.10 and the skewness $S\sigma$ (see figures 4.11-4.14).

Starting with the scaled variance, the largest baryon fluctuations are observed around $\Delta y = 1.0$, for very narrow windows, the fluctuations become Poissonian, and for the wide windows, conservation of baryon number contributes the prominent role. For the rest of the nuclear clusters i.e., proton, deuteron, triton, helium-3, and helium-4, one can observe a slight difference between two scenarios with the crossover having stronger effects. Overall, the proton number fluctuates less than the baryon number, as one might perceive, along with the slight differences between the two scenarios can be seen for the rest of the nuclear clusters which are not involved as a significant signal.

Next, we proceed to the skewness. Although the effects of the scaled variance which include participant fluctuations are prominently in active for all rapidity windows, we cannot observe explicit enhancements in the skewness of the free protons as well as the nuclear clusters in case of a phase transition for larger rapidity windows. Therefore, we propose that the skewness in a rapidity window of $\Delta y = 1.0$ is the most appropriate to observe any signals of a phase transition provided here.

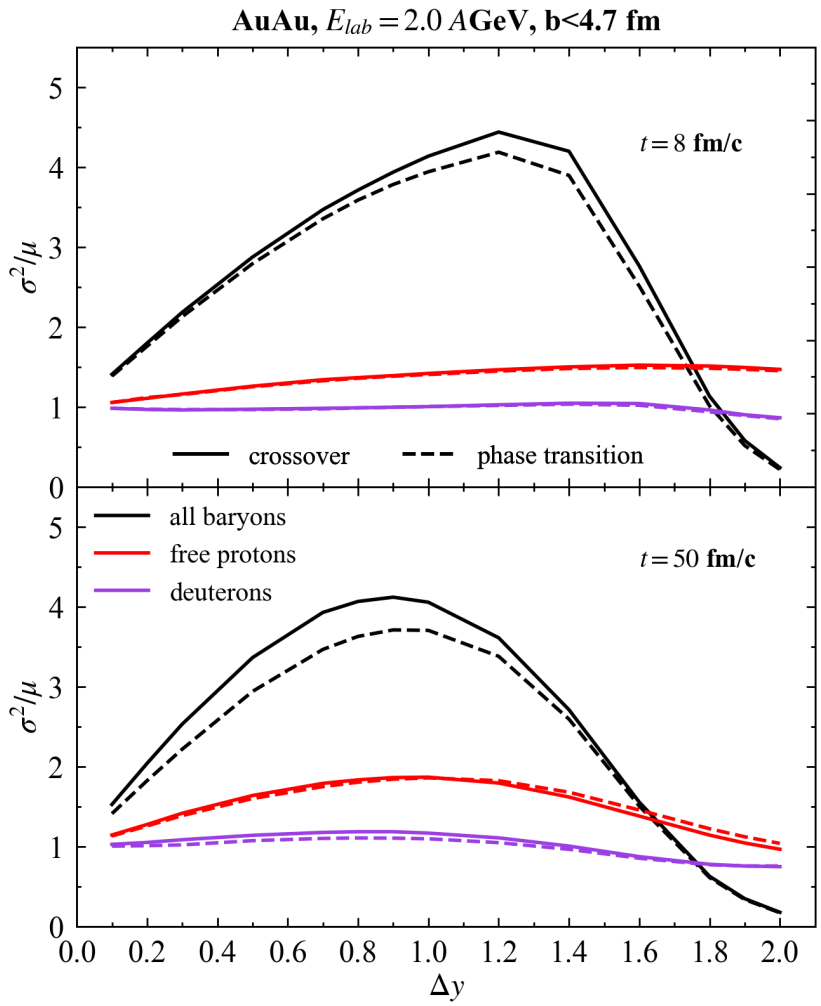


**Figure 4.7** Scaled variance as a function of rapidity window of the baryons (black), protons (red) and deuterons (purple) at the time 8 fm/c and 50 fm/c $E_{\text{lab}} = 2.0\ A$GeV

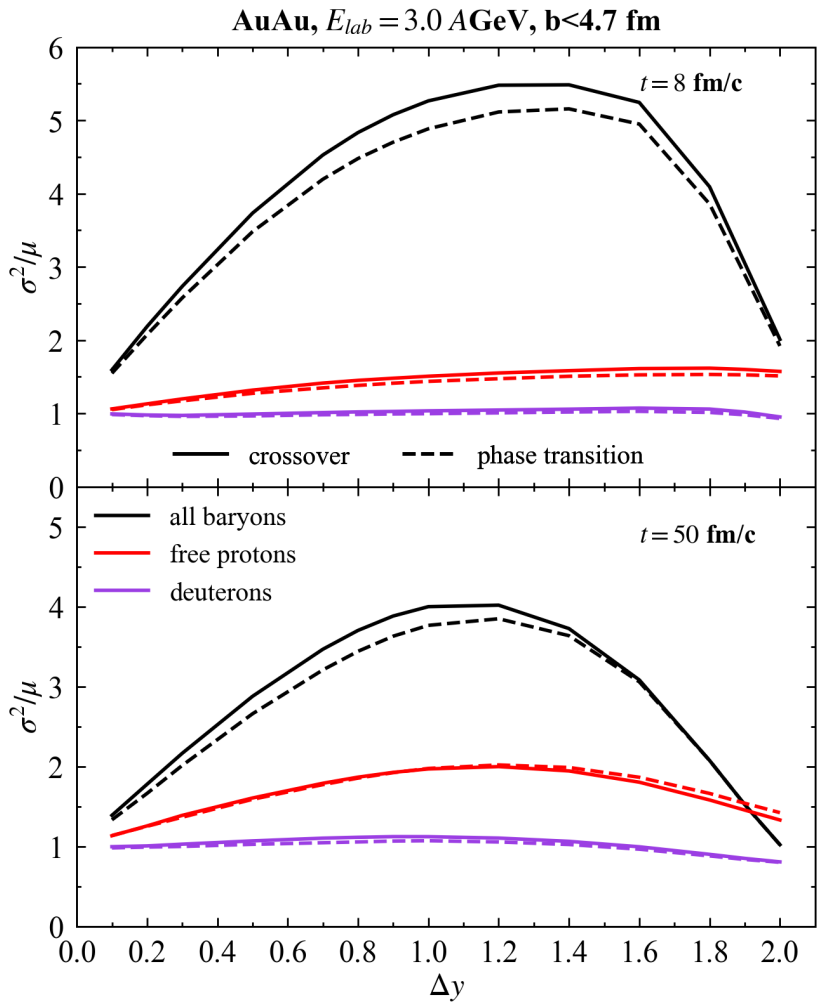


**Figure 4.8** Scaled variance as a function of rapidity window of the baryons (black), protons (red) and deuterons (purple) at the time 8 fm/c and 50 fm/c $E_{\text{lab}} = 3.0$ $A$GeV

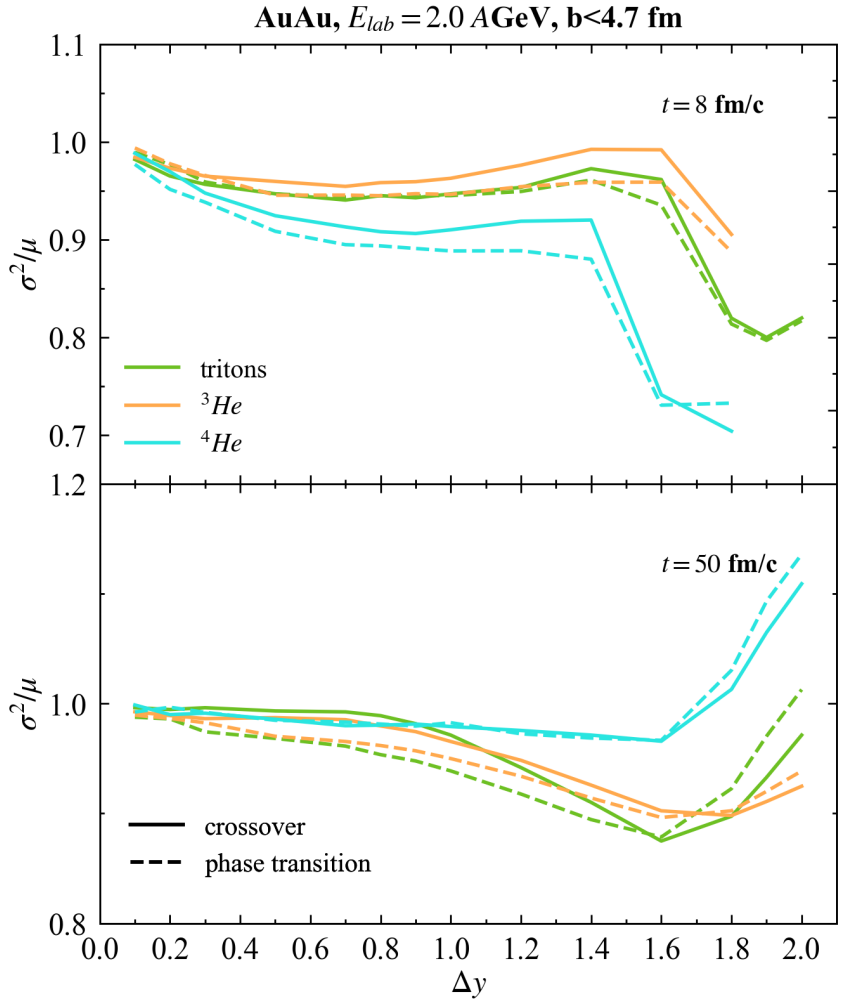


**Figure 4.9** Scaled variance as a function of rapidity window of tritons (green), $^3He$ (orange) and $^4He$ (blue) at the time 8 fm/c and 50 fm/c $E_{\text{lab}} = 2.0$ $A$GeV

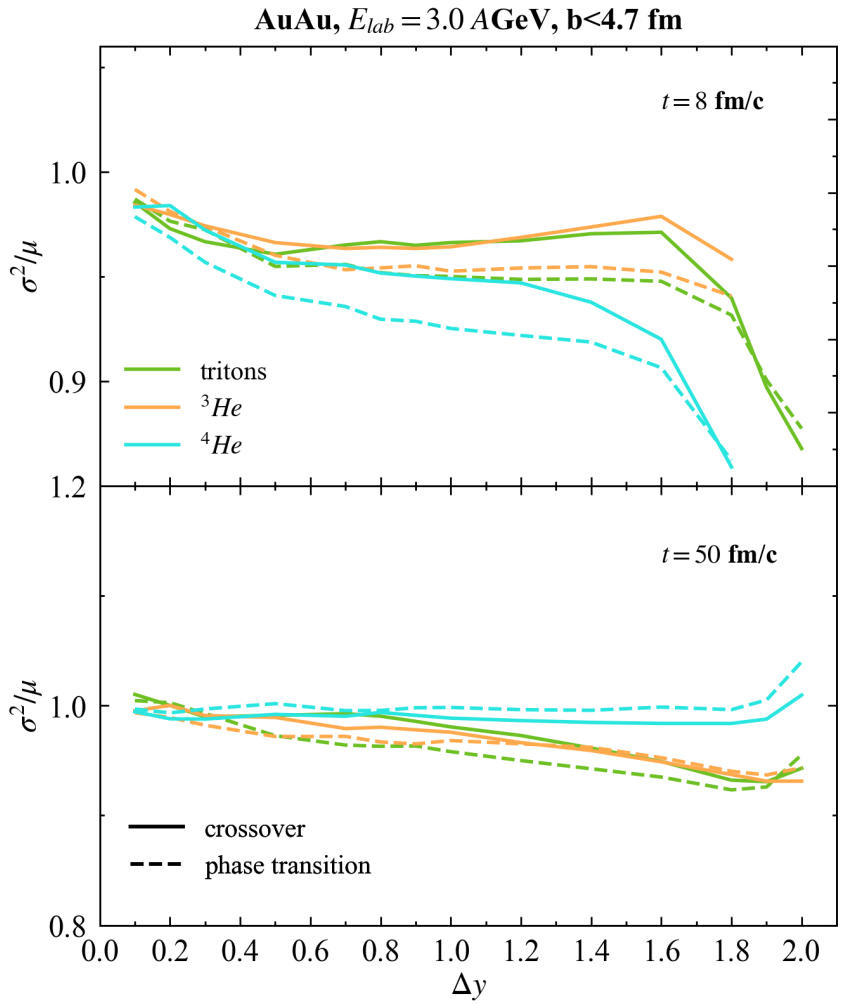


**Figure 4.10** Scaled variance as a function of rapidity window of tritons (green), $^3He$ (orange) and $^4He$ (blue) at the time 8 fm/c and 50 fm/c $E_{\text{lab}} = 3.0$ $A$GeV

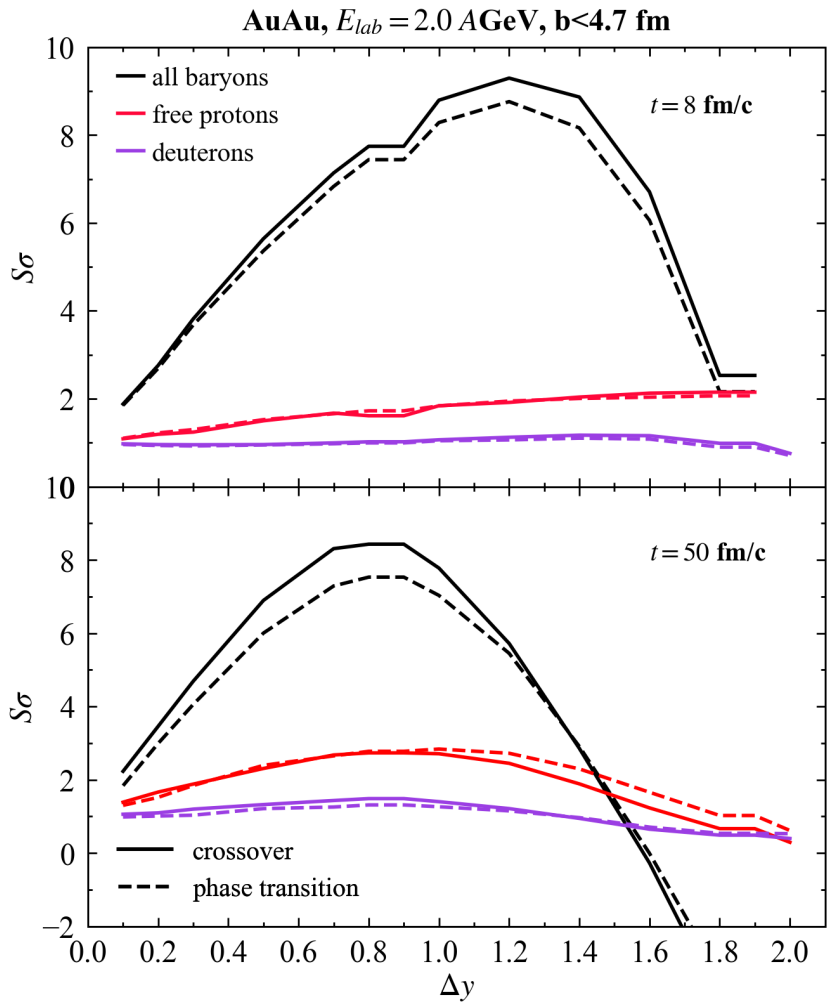


**Figure 4.11** $S\sigma$ as a function of rapidity window of the baryons (black), protons (red) and deuterons (purple) at the time 8 fm/c and 50 fm/c $E_{\text{lab}} = 2.0$ $A$GeV

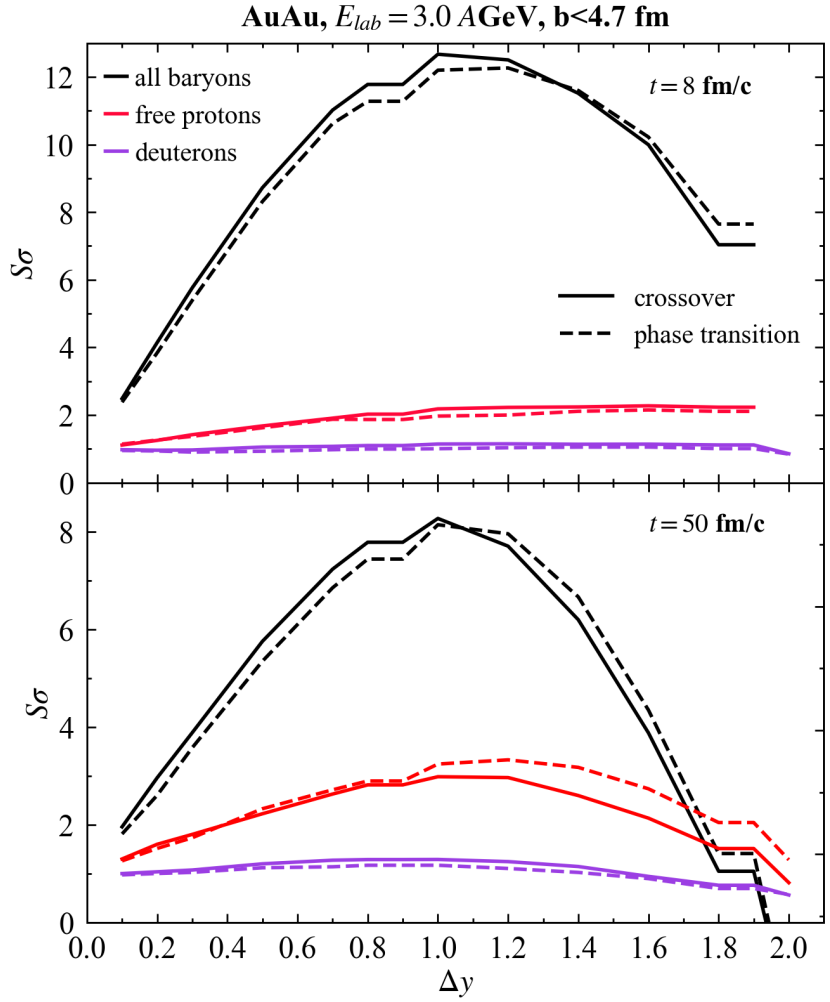


**Figure 4.12** $S\sigma$ as a function of rapidity window of the baryons (black), protons (red) and deuterons (purple) at the time 8 fm/c and 50 fm/c $E_{\text{lab}} = 3.0$ $A$GeV

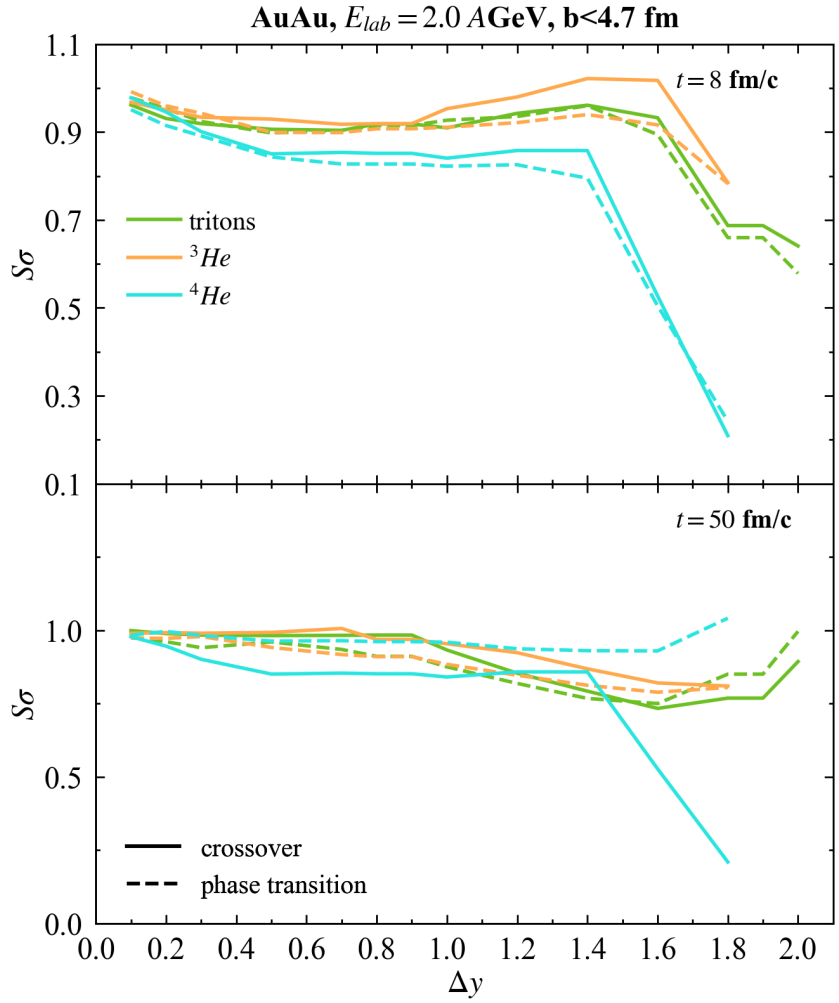


**Figure 4.13** $S\sigma$ as a function of rapidity window of tritons (green), $^3He$ (orange) and $^4He$ (blue) at the time 8 fm/c and 50 fm/c $E_{\text{lab}} = 2.0$ $A$GeV

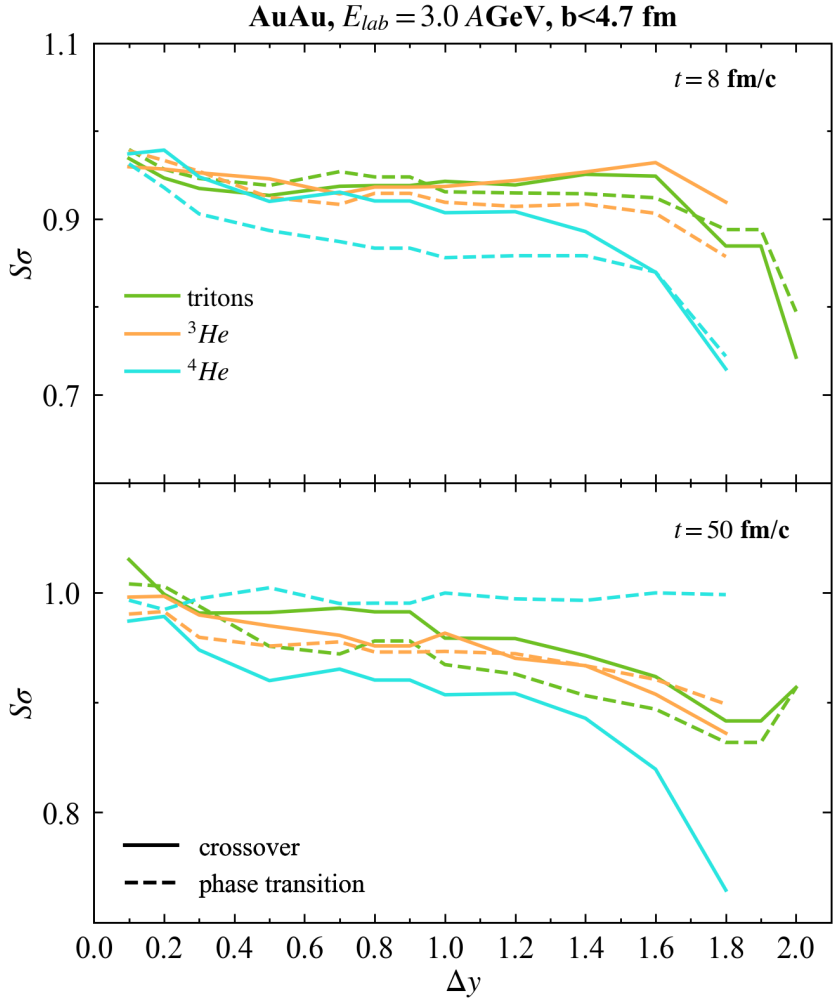


**Figure 4.14** $S\sigma$ as a function of rapidity window of tritons (green), $^3He$ (orange) and $^4He$ (blue) at the time 8 fm/c and 50 fm/c $E_{\text{lab}} = 3.0$ $A$GeV

After we are done observing the results with the rapidity window dependence, the upcoming section is going to represent how we confirm our calculations according to experimental data in a picture of actual collision picture via time evolution in light nuclei ratios.

## 4.4 Light nuclei ratios

After the comparison between the fluctuations in different rapidity windows, we can now treat the results as a confirmation that the phase transition will have a substantial impact to fluctuations of the baryon number in coordinate space (spatial volume). We can calculate the time dependence in the double ratios between the following particles: proton (p), deuteron (d), triton (t), helium-3 ($^3He$), and helium-4 ($^4He$). The double ratios are expressed as (STAR Collaboration, 2023)

$$\frac{(t)(p)}{d^2} \quad \text{and} \quad \frac{(^4He)(p)}{(^3He)(d)} \ . \tag{23}$$

These expressions in double ratios are useful since they eliminate the volume factor as the number of a certain nuclear cluster is calculated using the thermal model. Figures 4.15 and 4.16 display the time evolution in the ratios for corresponding beam energies in comparison between the results from coordinate space and momentum space.

For every curve, we observe that the ratios begin to rise until about $10$ fm/c, at which point a minor enhancement in the phase transition over the crossover occurs. Remarkably, for both examined beam energies, this is also readily apparent in the ratio $(N_{^4He} \times N_p)/(N_{^3He} \times N_d)$ determined in the rapidity window. In contrast, the cumulant ratio never displayed a distinct signal in momentum space. But all ratios eventually become close to the same value after a long enough period of time. The double ratios are also compared to the STAR experiment results at $E_{\text{lab}} = 3.0\ A$GeV (Abdulhamid et al., 2024) for completeness, and correspond well with the values obtained from our models for both equations of state at late times. In agreement with this, experimentally we can only observe these ratios at late times. Any peak structure or sudden modification is not visible due to the absence of further interactions as the system reaches its freeze-out state.

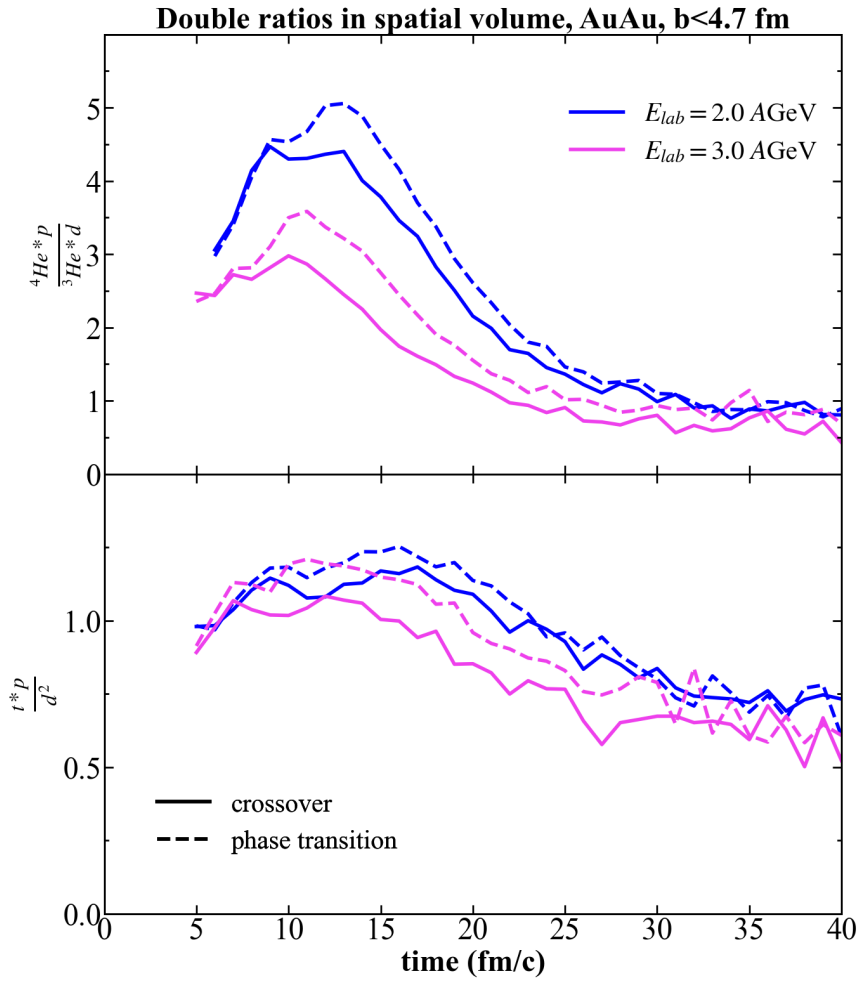


**Figure 4.15** Time evolution of double ratios $\frac{(t)(p)}{d^2}$ and $\frac{(He4)(p)}{(He3)(d)}$ for corresponding energies of $2.0\ A$GeV (blue) and $3.0\ A$GeV (pink) in coordinate space.

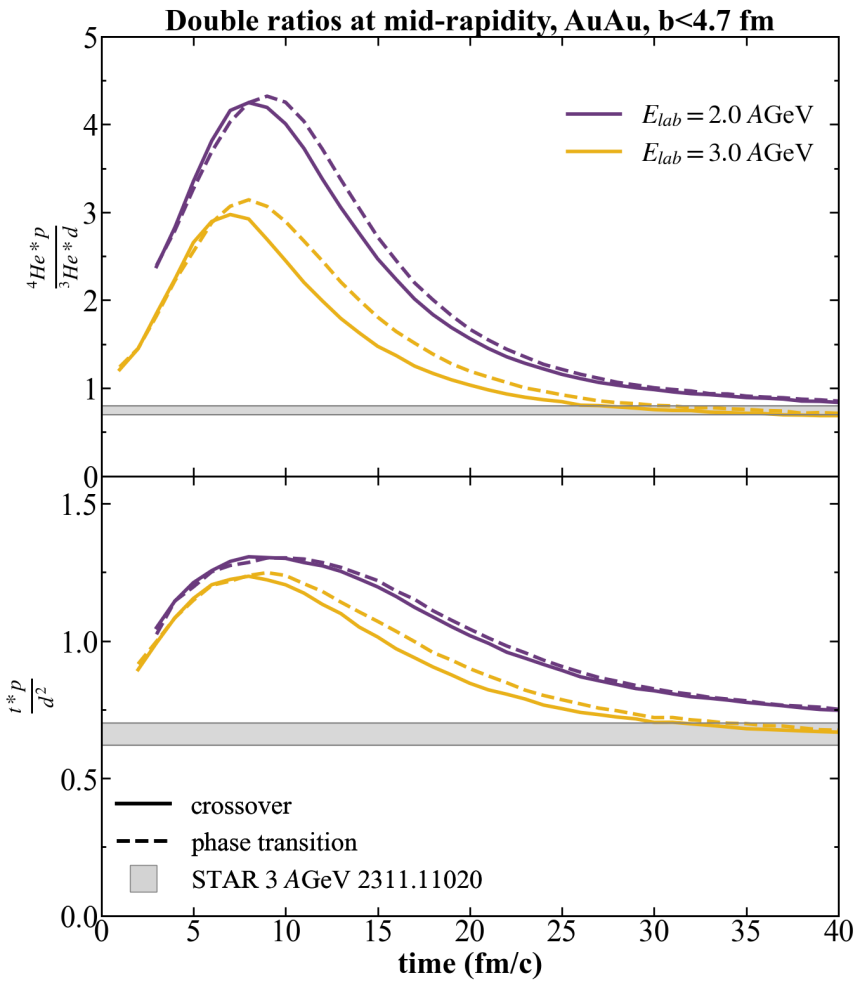


**Figure 4.16** Time evolution of double ratios $(t * p)/d^2$ and $(^4He * p)/(^3He * d)$ for corresponding energies of 2.0 $A$GeV (purple) and 3.0 $A$GeV (yellow) in momentum space. The gray bands correspond to the results from the STAR experiment of Au+Au at $E_{\text{lab}} = 3.0$ $A$GeV, $0 - 10\%$ centrality. The data is taken from figure 16 (b) in (Abdulhamid et al., 2024).